Primordial helium entrained by the hottest mantle plumes

M. G. Jackson[1], J. G. Konter[2] & T.W. Becker[3]

Helium isotopes provide an important tool for tracing early-Earth, primordial reservoirs that have survived in the planet's interior[1–3]. Volcanic hotspot lavas, like those erupted at Hawaii and Iceland, can host rare, high ^{3}He/^{4}He isotopic ratios (up to 50 times[4] the present atmospheric ratio, Ra) compared to the lower ^{3}He/^{4}He ratios identified in mid-ocean-ridge basalts that form by melting the upper mantle (about 8Ra; ref. 5). A long-standing hypothesis maintains that the high-^{3}He/^{4}He domain resides in the deep mantle[6–8], beneath the upper mantle sampled by mid-ocean-ridge basalts, and that buoyantly upwelling plumes from the deep mantle transport high-^{3}He/^{4}He material to the shallow mantle beneath plume-fed hotspots. One problem with this hypothesis is that, while some hotspots have ^{3}He/^{4}He values ranging from low to high, other hotspots exhibit only low ^{3}He/^{4}He ratios. Here we show that, among hotspots suggested to overlie mantle plumes[9,10], those with the highest maximum ^{3}He/^{4}He ratios have high hotspot buoyancy fluxes and overlie regions with seismic low-velocity anomalies in the upper mantle[11], unlike plume-fed hotspots with only low maximum ^{3}He/^{4}He ratios. We interpret the relationships between ^{3}He/^{4}He values, hotspot buoyancy flux, and upper-mantle shear wave velocity to mean that hot plumes—which exhibit seismic low-velocity anomalies at depths of 200 kilometres—are more buoyant and entrain both high-^{3}He/^{4}He and low-^{3}He/^{4}He material. In contrast, cooler, less buoyant plumes do not entrain this high-^{3}He/^{4}He material. This can be explained if the high-^{3}He/^{4}He domain is denser than low-^{3}He/^{4}He mantle components hosted in plumes, and if high-^{3}He/^{4}He material is entrained from the deep mantle only by the hottest, most buoyant plumes[12]. Such a dense, deep-mantle high-^{3}He/^{4}He domain could remain isolated from the convecting mantle[13,14], which may help to explain the preservation of early Hadean ($>$4.5 billion years ago) geochemical anomalies in lavas sampling this reservoir[1–3].

The Earth's mantle is chemically and isotopically heterogeneous[15–17], but the depth distribution and thermochemical dynamics governing the composition of the mantle are not well known. Basalts erupted at mid-ocean ridges, called MORB, are melts of the shallow upper mantle, and their geochemistry indicates that the upper mantle has experienced long-term stirring and geochemical depletion by melt extraction[1,15,16]. Additionally, MORB erupted far from hotspots exhibit relatively uniform ^{3}He/^{4}He values—with a median[5] of 8Ra ± 1Ra—that reflect the upper mantle's composition. In contrast, ocean island basalts erupted at many intraplate volcanic hotspots, thought to be melts of buoyantly upwelling mantle plumes originating in the deep mantle[18], erupt lavas with ^{3}He/^{4}He values that range[4,5,19] between about 5Ra and 50Ra. Whereas MORB results from passive melting of the shallow upper mantle, mantle plumes convey material from the deep mantle, and plume-fed hotspot volcanoes provide information about the composition of deep-mantle reservoirs sampled by plumes[15–17]. Indeed, hotspot lavas display more geochemically diverse compositions than do MORBs, and these compositions are grouped into several endmember compositions with different isotopic compositions (for example, ^{87}Sr/^{86}Sr, ^{143}Nd/^{144}Nd and ^{206}Pb/^{204}Pb)[15–17]. The generation of these endmembers is attributed to subduction of oceanic and continental lithosphere into the mantle, a process that contributes substantial chemical heterogeneity to the mantle over time[16,17]. These subducted materials are then sampled by buoyantly upwelling mantle plumes that melt beneath hotspots.

Hotspot lavas erupted at the Earth's surface also record the presence of a mantle plume component with primordial, high ^{3}He/^{4}He values[7,20,21] (Fig. 1 and Extended Data Fig. 1). Unlike the other mantle components, which are formed by subducted materials, this primordial component is 'least modified' by subducted materials over geologic time[17], and is thus a relatively pristine reservoir in the mantle. Geochemical signatures associated with the earliest history of the planet—including anomalous ^{129}Xe/^{130}Xe (ref. 1) and ^{182}W/^{184}W (ref. 2)—are identified in lavas with primitive, high ^{3}He/^{4}He values, which is consistent with the model that the mantle domain sampled by high-^{3}He/^{4}He lavas is early-formed and has preserved primordial geochemical characteristics for over 4.5 billion years[3]. An important question is where the early-formed high-^{3}He/^{4}He reservoir is located in the Earth's interior, given that the long-term preservation of this primordial geochemical signature requires isolation from mantle convection.

A long-standing hypothesis maintains that the high-^{3}He/^{4}He domain is located in the lower mantle, and volcanic hotspots that erupt lavas with high ^{3}He/^{4}He values are sourced by upwelling plumes[6–8]. Seismic techniques have identified plume conduits beneath hotspots[9,10,22], and this allows us to test for a relationship between high ^{3}He/^{4}He values and the presence of plumes beneath hotspots. Figures 1 and 2 show the maximum ^{3}He/^{4}He values for the 38 hotspots with available ^{3}He/^{4}He data. Figures 1 and 2 also indicate whether a plume[9,10] has been identified under each hotspot (Methods). It is important to note that lower ^{3}He/^{4}He values have also been measured at most of the hotspots shown in Fig. 1. For example, the hotspots with the highest maximum ^{3}He/^{4}He values ($>$30Ra)—Hawaii, Iceland, the Galapagos and Samoa—also have lavas with low ^{3}He/^{4}He values that overlap with, or extend below, the ^{3}He/^{4}He range in MORB (Methods). Thus, many hotspots that sample the primitive high-^{3}He/^{4}He domain also sample low-^{3}He/^{4}He mantle domains composed of recycled lithosphere and depleted MORB mantle.

However, only the highest ^{3}He/^{4}He value identified at each hotspot is shown in the figures. This is because the primary goal of this study is to evaluate the most primitive, highest-^{3}He/^{4}He component sampled at each hotspot, not to determine the distribution of low ^{3}He/^{4}He values, which reflect contributions from non-primordial recycled lithosphere and depleted MORB mantle components (Methods). However, in two cases the highest ^{3}He/^{4}He value occurs early in the history of the hotspot during the flood basalt stage (that is, the Afar–Ethiopian Rift

[1]University of California Santa Barbara, Department of Earth Science, Santa Barbara, California 93106-9630, USA. [2]Department of Geology and Geophysics, School of Ocean and Earth Science and Technology, University of Hawaii, Manoa, 1680 East–West Road, Honolulu, Hawaii 96822, USA. [3]Jackson School of Geosciences, University of Texas at Austin, 1 University Station, C1160, Austin, Texas 78712-0254, USA.
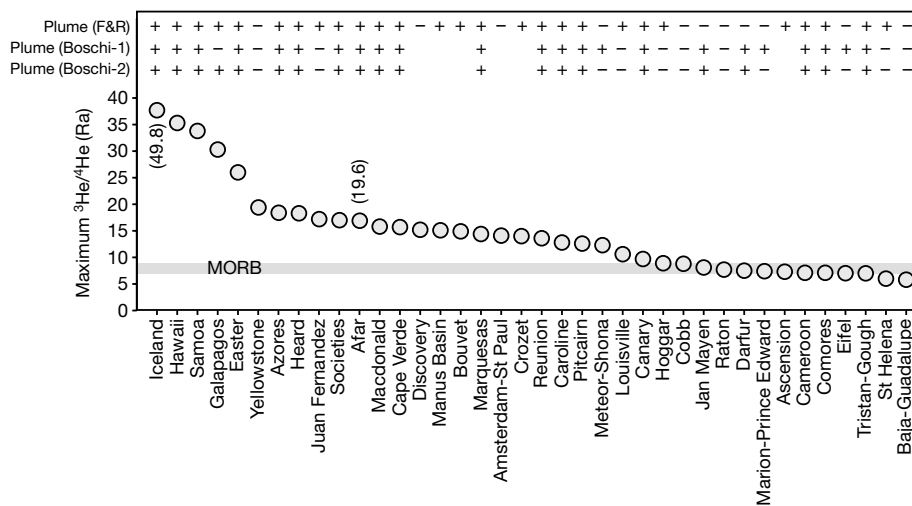
Figure 1 | The maximum ^{3}He/^{4}He values at 38 hotspots organized in order of decreasing maximum ^{3}He/^{4}He. See Supplementary Table 1. Three plume catalogues are shown here—the French and Romanowicz[9] model ('F&R'), Boschi et al.'s[10] seismology-based plume extent using SMEAN[25] ('Boschi-1'), and the average plume extent of five different models ('Boschi-2'). If a plume has been identified under a hotspot from one of these catalogues, a plus symbol is shown at the top of the figure (see Methods); if no plume is identified, a minus symbol is shown; if the presence of a plume was not evaluated, no symbol is shown. Plumes corresponding to the Boschi-1 catalogue are shown in Figs 2 and 3; the Boschi-2 catalogue is also used in Fig. 3. The three plume catalogues are used to identify plume-related and non-plume hotspots in Extended Data Figs 1–3. Higher ^{3}He/^{4}He values (in parentheses) are associated with the earliest stages of volcanism at the Iceland and Afar hotspots, but are not used in the analysis (see Methods).

system; the Iceland–Baffin Island–West Greenland system), a more recently erupted lava with a somewhat lower ^{3}He/^{4}He value is used (as explained in the Methods and Supplementary Table 1, which contains the source data for all figures).

Hotspots with high maximum ^{3}He/^{4}He values tend to be associated with plumes (Fig. 1 and Methods). For example, the five hotspots with the highest ^{3}He/^{4}He values—Iceland, Hawaii, Samoa, the Galapagos, and Easter—are associated with plumes in at least two of the three different plume catalogues[9,10]. However, a key observation is that not all hotspots overlying plumes have high ^{3}He/^{4}He. Three hotspots—Cameroon, Comores and Tristan-Gough—which are associated with plumes in all the plume catalogues, each have a maximum ^{3}He/^{4}He value that overlaps with that of MORB (Fig. 1), indicating that these plume-fed hotspots sample only low-^{3}He/^{4}He recycled lithosphere or depleted MORB mantle. An important question is why this is the case.

One hypothesis is that higher-^{3}He/^{4}He material is sampled by hotter plumes because hotter, more thermally buoyant plumes entrain a greater fraction of high-^{3}He/^{4}He material from the deep mantle than cooler plumes, which exhibit only low ^{3}He/^{4}He values[23]. Indeed, petrological thermometers suggest that hotter hotspots have higher maximum ^{3}He/^{4}He values[23], and that these high-^{3}He/^{4}He hotspots are associated with higher hotspot buoyancy fluxes[5,12,23]. Additionally, hotspots with Sr, Nd and Pb radiogenic isotopic compositions most similar to the mantle C ("Common")[21] component—the one presumed to host material with elevated ^{3}He/^{4}He values—overlie regions of mantle with anomalously slow seismic shear-wave velocity (attributed to higher mantle temperatures) at a depth of 200 km compared to hotspot compositions with a weaker C contribution[11]. Konter and Becker[11] proposed that direct comparison of hotspot ^{3}He/^{4}He and shear-wave anomalies should be used to evaluate this observation further. Therefore, we here provide comparison of maximum ^{3}He/^{4}He and shear-wave anomalies in the shallow upper mantle beneath hotspots. Additionally, comparison of maximum ^{3}He/^{4}He values with recent hotspot buoyancy flux estimates[24] provides an additional constraint on the origin of the high-^{3}He/^{4}He component sampled at hotspots.

We compare the maximum ^{3}He/^{4}He value at each plume-related hotspot with shear-wave velocity anomalies in the upper mantle (at 200 km depth) to test whether hotter mantle plumes, which are expected to have lower seismic velocities at depth, have higher maximum ^{3}He/^{4}He values (Fig. 3 and Extended Data Fig. 2; Methods). We use an updated variant of a global composite shear-wave model (SMEAN)[25] for our analysis because it captures the most common, robust, long-wavelength structure across different models (Methods). We also explore whether maximum ^{3}He/^{4}He values relate to seismic velocities by using a suite of individual seismic models (Methods). Using three previously published

plume catalogues[9,10] (Fig. 1 and Methods), we evaluate the correlation of maximum ^{3}He/^{4}He values with seismic velocity anomalies for plume-fed hotspots, those inferred to not be related to plumes, and the complete catalogue (Fig. 3 and Extended Data Fig. 2). We also compare maximum ^{3}He/^{4}He values at each hotspot with buoyancy flux estimates[24] (Fig. 3 and Extended Data Fig. 3). Although the relationship between ^{3}He/^{4}He and hotspot buoyancy flux has been explored before[5], Fig. 3 and Extended Data Fig. 3 evaluate this relationship in the light of expanded ^{3}He/^{4}He datasets (Supplementary Table 1) and new buoyancy flux estimates[24]. Compared to plume-fed hotspots with lower maximum ^{3}He/^{4}He values, plume-fed hotspots with higher maximum ^{3}He/^{4}He values tend to have higher hotspot buoyancy fluxes and lower shear-wave velocities at 200 km depth (Fig. 3). This relationship holds for different definitions of plumes[9,10] and for most global seismic models (Fig. 3 and Extended Data Figs 2 and 3; Methods). Note that the Pearson correlation coefficients for these relationships (that is, between ^{3}He/^{4}He, SMEAN2 seismic shear-wave velocities, and buoyancy flux) vary slightly depending on the plume catalogue used. For example, if the Boschi-1 plume catalogue[10] is used (see Fig. 1 for definition of plume
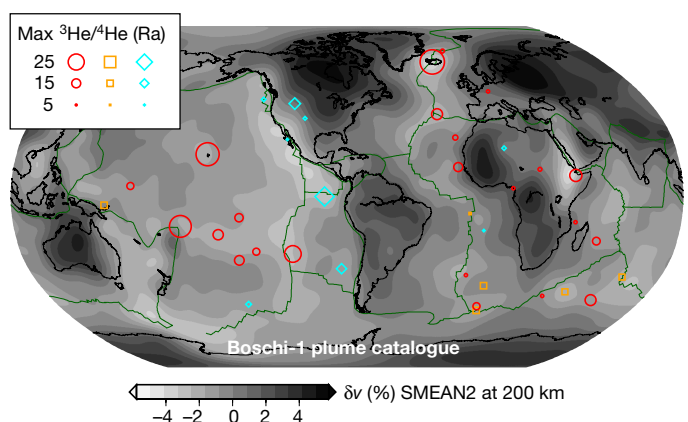

Figure 2 | Map showing the maximum ^{3}He/^{4}He values at global hotspots. ^{3}He/^{4}He data are from Fig. 1. The magnitude of maximum ^{3}He/^{4}He data from plume-fed (red circles) and non-plume-fed (cyan diamonds) hotspots are shown; hotspots not evaluated for the presence of a plume are also shown (orange squares) (see Supplementary Table 1). The Boschi-1 plume catalogue[10] (Fig. 1) is used to determine whether a hotspot is associated with a plume; see Extended Data Fig. 1 for equivalent figures that use different plume catalogues (that is, the F&R and Boschi-2 catalogues from Fig. 1). The background of the map is contoured (greyscale) for seismic shear-wave velocity anomalies at 200 km using the SMEAN2[25] model (Methods).
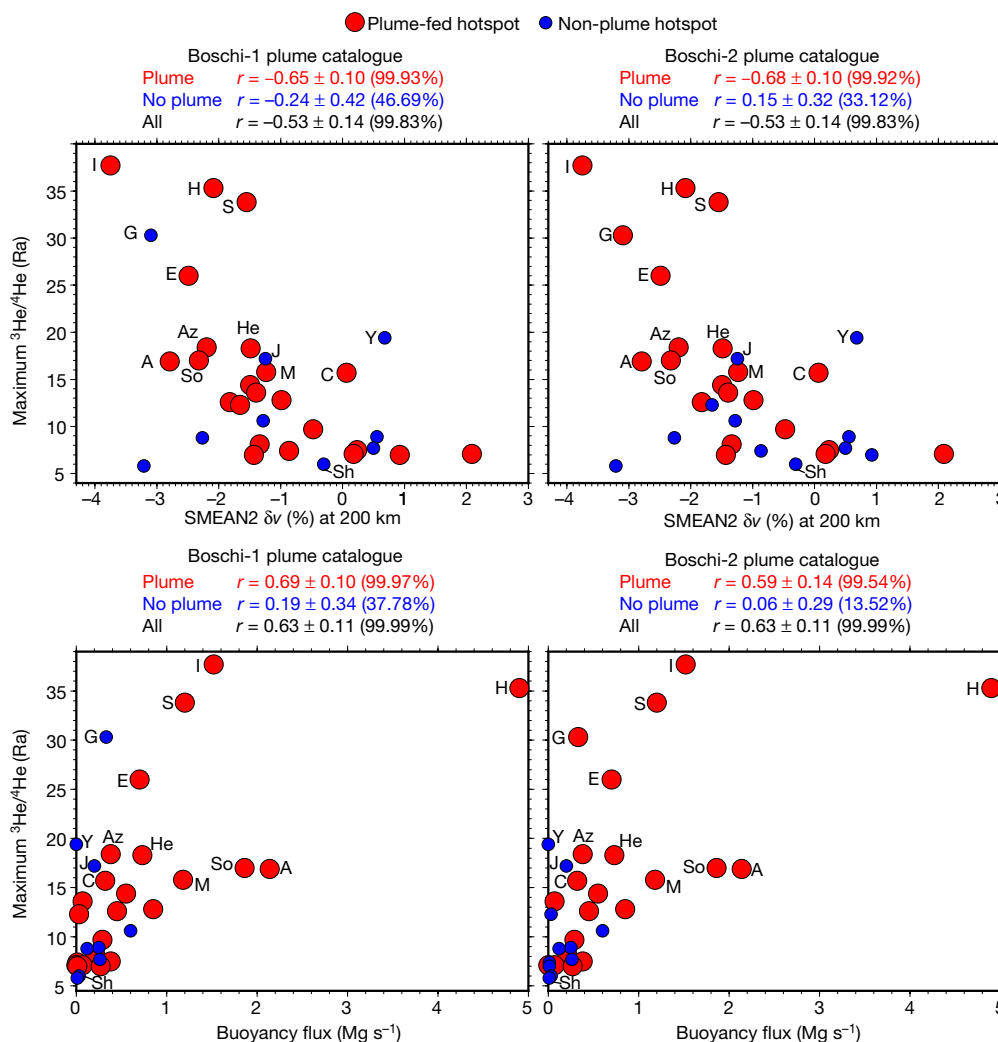
Figure 3 | Maximum ³He/⁴He values at plume-fed hotspots compared with seismic shear-wave velocity anomalies at 200 km and with hotspot buoyancy flux. ³He/⁴He data is from Fig. 1. The presence or absence of a plume is evaluated using two plume catalogues, Boschi-1 (left panels) and Boschi-2 (right panels)[10]; the F&R[9] plume catalogue is used to separate plume-fed and non-plume-fed hotspots in Extended Data Figs 2 and 3 (see plume catalogue definitions in Fig. 1). The Pearson correlation coefficients r are provided in the panels and are calculated from individual observations for plume-fed hotspots (for the red symbols only), non-plume-fed hotspots (blue symbols only), and all hotspots; in order to evaluate the actual statistical relevance of the correlations, the 1σ uncertainty is provided (calculated using bootstrap), as is the significance level of the correlation coefficients (P value in parentheses,

calculated with Student's t-test assuming normally distributed data). The sample sizes for the Boschi-1 and Boschi-2 plume catalogues are as follows: Boschi-1 ($n = 23$ plumes, $n = 9$ non-plumes); Boschi-2 ($n = 21$ plumes, $n = 11$ non-plumes). See Methods for discussion of the SMEAN2 seismic model. The hotspot buoyancy flux (MiFil volume method) is from ref. 24 (bottom panels). The maximum ³He/⁴He values at hotspots are also compared with shear-wave velocity anomalies (δv) (top panels). Additional seismic models and different hotspot buoyancy flux estimates are compared with maximum ³He/⁴He in Extended Data Figs 2 and 3. See Supplementary Table 1 for data shown here. H = Hawaii, I = Iceland, S = Samoa, G = Galapagos, E = Easter, Y = Yellowstone, A = Afar, So = Societies, C = Cape Verde, Az = Azores, M = Macdonald, He = Heard, J = Juan Fernandez, Sh = St Helena.

catalogues), the correlation coefficient between ³He/⁴He and SMEAN2 seismic shear-wave velocity anomalies ($r = -0.65$; Fig. 3) is slightly worse than if the Boschi-2 plume catalogue[10] ($r = -0.68$; Fig. 3) or the French and Romanowicz plume catalogue[9] ($r = -0.67$; Extended Data Fig. 2) is used.

If the temperature of a plume relates to the efficiency of entrainment of material from a deep-mantle, high-³He/⁴He reservoir, then shallow-sourced hotspots (that is, not sourced by deep-mantle plumes) are not expected to exhibit correlations between maximum ³He/⁴He values and seismic velocity anomalies or buoyancy fluxes. Both seismic shear-wave velocity anomaly and buoyancy flux correlations with ³He/⁴He are indeed weaker if the whole hotspot catalogue is considered rather than plumes only, and correlations break down for the non-plume-fed hotspots (Fig. 3 and Extended Data Figs 2 and 3).

We limit comparison of maximum ³He/⁴He values with shear-wave anomalies at 200 km for two reasons. First, the relationship between

maximum ³He/⁴He values and seismic anomalies beneath plume-related hotspots is clear only in the shallow upper mantle. Second, previously identified relationships[11] between Sr, Nd and Pb isotopic signatures of the high-³He/⁴He mantle C component and shear-wave velocity at 200 km suggests that this depth interval provides a critical point of comparison. We do not interpret the strong relationship between maximum ³He/⁴He values and shear-wave velocity in the shallow mantle to mean that the high-³He/⁴He reservoir is located in the upper mantle, because this would predict that mid-ocean ridges sampling the upper mantle would have high ³He/⁴He values, which is not observed. Instead, we argue that shear-wave velocity differences between hotter and cooler plumes are amplified in the shallow mantle, possibly owing to enhanced partial melting (in a volatile-rich astheno-sphere) associated with the hottest plumes.

Some hotspots associated with seismically resolved plume conduits have maximum ³He/⁴He values that do not exceed the MORB range,

and if the low maximum $^3He/^4He$ values measured at these localities are representative, then high $^3He/^4He$ values do not appear to be required as a geochemical signature for deep-mantle plumes[26]. If this hypothesis is valid, then domains with low $^3He/^4He$ are heterogeneously distributed with domains of primordial high-$^3He/^4He$ material in the deep mantle sampled by plumes[27]. This may explain why plumes that exhibit high maximum $^3He/^4He$ values can also sample low-$^3He/^4He$ material[26] associated with depleted mantle or recycled lithosphere. The presence of recycled lithosphere in plumes would be consistent with the suggestion that seismically resolved plumes are not just thermal anomalies, but may be thermochemical features[9,28].

The results of this study suggest that the temperature, and therefore the effective buoyancy of a mantle plume, is related to whether high-$^3He/^4He$ material is entrained from the heterogeneous deep-mantle plume source (Fig. 3): the maximum $^3He/^4He$ values at plume-fed hotspots exhibit a positive correlation with hotspot buoyancy flux and an inverse relationship with seismic anomalies (and thus maximum $^3He/^4He$ has an inferred positive correlation with mantle temperature). Previous results showed that a deep, dense high-$^3He/^4He$ domain will be preferentially entrained by the hottest, most buoyant mantle plumes[12], but the details of the interplay between entrainment dynamics and isotope distributions remain unclear. The high-$^3He/^4He$ domain is predicted to be Fe-rich and dense if it formed by differentiation of an early, deep magma ocean[29]. If the high-$^3He/^4He$ mantle domain has a higher density than low-$^3He/^4He$ material, then cooler plumes with reduced thermal buoyancy will be capable of entraining only the relatively less dense, low-$^3He/^4He$ material (not the more dense, high-$^3He/^4He$ material). This model helps to explain the observation of low hotspot buoyancy and high shear-wave velocity anomalies (at 200 km depth) at plume-fed hotspots with low maximum $^3He/^4He$ values. In contrast, the hottest, most buoyant plumes will entrain both lower density, low-$^3He/^4He$ material and higher density, high-$^3He/^4He$ material. As a result, the hottest plumes can host a range of $^3He/^4He$ values, from low to high $^3He/^4He$ (Methods), which is what is observed at hotspots with the highest maximum $^3He/^4He$.

A deep, dense high-$^3He/^4He$ reservoir will also serve to preserve this mantle domain for long timescales, and can help to explain the presence of Hadean $^{129}Xe/^{130}Xe$ (ref. 1) and $^{182}W/^{184}W$ (ref. 2) signatures, and primitive Pb-isotopic compositions[3], in high-$^3He/^4He$ lavas. Dense reservoirs are resilient to entrainment into the convecting mantle, particularly in the lower mantle, where the higher viscosity (compared to the upper mantle) reduces the convective motions that attenuate primordial geochemical signatures[13,14,28]. High-density domains are inferred to exist in the deep mantle[14], and they may preserve primordial geochemical signatures, including high $^3He/^4He$ values, over geologic timescales[29,30]. Our results imply that many hotspots are indeed plume-fed, and the hottest, most buoyant plumes sample deep-mantle primordial domains. Furthermore, these results suggest how helium isotopic ratios, plume flux and upper mantle seismic shear-wave velocity anomalies can provide a quantitative link between surface magmatism and the thermo-chemical evolution of the Earth's mantle.

Online Content Methods, along with any additional Extended Data display items and Source Data, are available in the online version of the paper; references unique to these sections appear only in the online paper.

1. Mukhopadhyay, S. Early differentiation and volatile accretion recorded in deep-mantle neon and xenon. *Nature* **486,** 101–104 (2012).
2. Rizo, H. *et al.* Memories of Earth formation in the modern mantle: W isotopic compositions of flood basalt lavas. *Science* **352,** 809–812 (2016).
3. Jackson, M. G. *et al.* Evidence for the survival of the oldest terrestrial mantle reservoir. *Nature* **466,** 853–856 (2010).
4. Stuart, F. M., Lass-Evans, S., Fitton, J. G. & Ellam, R. M. High $^3He/^4He$ ratios in picritic basalts from Baffin Island and the role of a mixed reservoir in mantle plumes. *Nature* **424,** 57–59 (2003).
5. Graham, D. W. in *Noble Gases in Geochemistry and Cosmochemistry* (eds Porcelli, D., Ballentine, C. J. & Wieler, R.), *Rev. Mineral. Geochem.* Vol. 47, 247–318 (Mineralogical Society of America, 2002).
6. Allègre, C. J., Staudacher, T., Sarda, P. & Kurz, M. D. Constraints on evolution of Earth's mantle from rare gas systematics. *Nature* **303,** 762–766 (1983).
7. Hart, S. R., Hauri, E. H., Oschmann, L. A. & Whitehead, J. A. Mantle plumes and entrainment: isotopic evidence. *Science* **256,** 517–520 (1992).
8. Class, C. & Goldstein, S. L. Evolution of helium isotopes in the Earth's mantle. *Nature* **436,** 1107–1112 (2005).
9. French, S. W. & Romanowicz, B. Broad plumes rooted at the base of the Earth's mantle beneath major hotspots. *Nature* **525,** 95–99 (2015).
10. Boschi, L., Becker, T. W. & Steinberger, B. Mantle plumes: Dynamic models and seismic images. *Geochem. Geophys. Geosyst.* **7,** Q10006 (2007).
11. Konter, J. G. & Becker, T. W. Shallow lithospheric contribution to mantle plumes revealed by integrating seismic and geochemical data. *Geochem. Geophys. Geosyst.* **13,** Q02004 (2012).
12. Jellinek, A. M. & Manga, M. Links between long-lived hotspots, mantle plume, D″, and plate tectonics. *Rev. Geophys.* **42,** RG3002 (2004).
13. Samuel, H. & Farnetani, C. G. Thermochemical convection and helium concentrations in mantle plumes. *Earth Planet. Sci. Lett.* **207,** 39–56 (2003).
14. Garnero, E. J., McNamara, A. K. & Shim, S.-H. Continent-sized anomalous zones with low seismic velocity at the base of Earth's mantle. *Nat. Geosci.* **9,** 481–489 (2016).
15. Zindler, A. & Hart, S. Chemical geodynamics. *Annu. Rev. Earth Planet. Sci.* **14,** 493–571 (1986).
16. Hofmann, A. W. Mantle geochemistry: the message from oceanic volcanism. *Nature* **385,** 219–229 (1997).
17. White, W. M. Isotopes, DUPAL, LLSVPs, and Anekantavada. *Chem. Geol.* **419,** 10–28 (2015).
18. Morgan, W. J. Convection plumes in the lower mantle. *Nature* **230,** 42–43 (1971).
19. Class, C., Goldstein, S. L., Stute, M., Kurz, M. D. & Schlosser, P. Grand Comore Island: a well-constrained low $^3He/^4He$ mantle plume. *Earth Planet. Sci. Lett.* **233,** 391–409 (2005).
20. Farley, K. A., Natland, J. H. & Craig, H. Binary mixing of enriched and undegassed (primitive?) mantle components (He, Sr, Nd, Pb) in Samoan lavas. *Earth Planet. Sci. Lett.* **111,** 183–199 (1992).
21. Hanan, B. B. & Graham, D. W. Lead and helium isotope evidence from oceanic basalts for a common deep source of mantle plumes. *Science* **272,** 991–995 (1996).
22. Montelli, R., Nolet, G., Dahlen, F. A. & Masters, G. A catalogue of deep mantle plumes: New results from finite-frequency tomography. *Geochem. Geophys. Geosyst.* **7,** Q11007 (2006).
23. Putirka, K. Excess temperatures at ocean islands: implications for mantle layering and convection. *Geology* **36,** 283–286 (2008).
24. King, S. D. & Adam, C. Hotspot swells revisited. *Phys. Earth Planet. Inter.* **235,** 66–83 (2014).
25. Becker, T. W. & Boschi, L. A comparison of tomographic and geodynamic mantle models *Geochem. Geophys. Geosyst.* **3,** 1003 (2002).
26. Williams, C. D., Li, M., McNamara, A. K., Garnero, E. J. & van Soest, M. C. Episodic entrainment of deep primordial mantle material into ocean island basalts. *Nat. Commun.* **6,** 8937 (2015).
27. Li, M., McNamara, A. K. & Garnero, E. J. Chemical complexity of hotspots caused by cycling oceanic crust through mantle reservoirs. *Nat. Geosci.* **7,** 366–370 (2014).
28. Lin, S.-C. & van Keken, P. E. Dynamics of thermochemical plumes: 2. Complexity of plume structures and its implications for mapping mantle plumes. *Geochem. Geophys. Geosyst.* **7,** Q03003 (2006).
29. Coltice, N., Moreira, M., Hernlund, J. & Labrosse, S. Crystallization of a basal magma ocean recorded by helium and neon. *Earth Planet. Sci. Lett.* **233,** 391–409 (2005).
30. Deschamps, F., Kaminski, E. & Tackley, P. J. A deep mantle origin for the primitive signature of ocean island basalt. *Nat. Geosci.* **4,** 879–882 (2011).

Supplementary Information is available in the online version of the paper.

Author Contributions All authors contributed equally to the manuscript.

Author Information Reprints and permissions information is available at www.nature.com/reprints. The authors declare no competing financial interests. Readers are welcome to comment on the online version of the paper. Correspondence and requests for materials should be addressed to M.G.J. (jackson@geol.ucsb.edu).

METHODS

Defining the hotspot database. The hotspots explored in this paper represent the subset of hotspots from global hotspot compilations[31,32] that have existing ^{3}He/^{4}He data. Thus, a number of hotspots (Line Islands, Foundation and so on) are not included in our analysis because, to our knowledge, they have no existing ^{3}He/^{4}He data. To the treatment of global hotspots, we add the Manus Basin, which has ^{3}He/^{4}He data and an associated mantle plume[9,33]. We also add the Amsterdam–St Paul Islands, which have ^{3}He/^{4}He data[34]. Additional modifications to the hotspot databases of refs 31 and 32 are outlined in Supplementary Table 1. In total, 38 hotspots are represented in the database shown in the Supplementary Table 1.

Selection of extreme high ^{3}He/^{4}He lavas from each hotspot. The 38 hotspots in the database shown in Fig. 1 (see Supplementary Table 1) have been characterized for ^{3}He/^{4}He. The database includes hotspots from both oceanic and continental settings. With two exceptions (see below), in the database we include only the maximum ^{3}He/^{4}He ratio reported from each hotspot locality. The reported ^{3}He/^{4}He data were measured in magmatic phases or volcanic glass, with one exception: at the Eifel hotspot, the only available ^{3}He/^{4}He data were obtained on mantle xenoliths, but the ^{3}He/^{4}He ratios from xenoliths are suggested to be in equilibrium with the host lavas[35]. Care was taken to select ^{3}He/^{4}He measurements that are the most likely to reflect the primary magmatic values from the hotspot.

Although the ^{3}He/^{4}He values recorded in Supplementary Table 1 reflect maximum magmatic values at each hotspot, in two cases—the Afar hotspot and the Iceland hotspot—^{3}He/^{4}He values that are lower than the maximum values at the respective hotspot are used. At the Iceland hotspot, the highest ^{3}He/^{4}He values (up to 49.8Ra) are associated with the flood basalt stage of the early Iceland plume[4,36,37]. However, the anomalously high plume flux of the palaeo-Iceland plume cannot directly be related to the seismic properties, which reflect the modern Iceland plume. Therefore, a lower ^{3}He/^{4}He value (37.7Ra) associated with more recently erupted lavas[38] are used in our analysis. Similarly, a higher ^{3}He/^{4}He value (19.6Ra) from the Afar hotspot is available, but was erupted early in the history (that is, the Oligocene) of the hotspot. Therefore, a more recently erupted lava with a lower ^{3}He/^{4}He (16.9Ra) is used for the Afar hotspot[39–41].

We compile only the maximum ^{3}He/^{4}He at hotspots, but the variability in magmatic ^{3}He/^{4}He in lavas at a given hotspot can be substantial. For example, the hotspots with the highest maximum ^{3}He/^{4}He values (>20Ra), including Hawaii[42–45], Iceland[33,38,46], Galapagos[47–49], Samoa[20,50,51], and Easter[52,53] all have a wide range of ^{3}He/^{4}He values that extend down to (or below) MORB-like values. However, this study does not focus on the lower ^{3}He/^{4}He values measured at hotspots. Low-^{3}He/^{4}He mantle components—including DMM (depleted MORB mantle)[5], EM1 (enriched mantle 1)[54,55], EM2 (enriched mantle 2)[50,56] and HIMU (high $\mu = {}^{238}$U/^{204}Pb)[57–60]—represent upper mantle (DMM) or recycled lithospheric materials (EM1, EM2 and HIMU) that have low ^{3}He/^{4}He values that overlap with MORB or extend to sub-MORB values. Unlike high ^{3}He/^{4}He values, low ^{3}He/^{4}He values in mantle-derived lavas are not indicative of a specific mantle component, but instead are characteristic of a suite of low-^{3}He/^{4}He components with different origins (DMM, EM1, EM2 and HIMU), and the relation of these low-^{3}He/^{4}He endmembers to seismic models was assessed by ref. 11. Therefore, this study focuses only on the highest ^{3}He/^{4}He value at each hotspot: a compilation of low ^{3}He/^{4}He values in hotspots is not useful to the primary goal of this study, which is to evaluate the database of the highest, most primitive ^{3}He/^{4}He ratios sampled by hotspots globally and relate these isotopic compositions to geophysical observables. We acknowledge that higher ^{3}He/^{4}He values may exist at the hotspot localities examined here, and future work may encounter even higher ^{3}He/^{4}He values than shown in Fig. 1. Nonetheless, the existing data set allows us to make new observations regarding the relationship between maximum ^{3}He/^{4}He in lavas erupted at the surface, hotspot buoyancy flux, and seismic anomalies at a depth of 200 km.

Identifying which hotspots are sourced by plumes. We distinguish between plume-fed and non-plume-fed hotspots when comparing maximum ^{3}He/^{4}He values with hotspot buoyancy flux and seismic anomalies in the mantle beneath hotspots. We use three different plume catalogues for this purpose. These three catalogues provide a means of independently evaluating the presence or absence of plumes under hotspots.

A seismic definition for mantle plumes was developed by Boschi et al.[10]. They quantify the degree of continuity of a plume from the base of the lower mantle to the shallow upper mantle based on seismic tomography using a value referred to as the normalized vertical extent (NVE). An NVE value of zero indicates no continuous vertical plume, and an NVE value of unity indicates that the plume is continuous throughout the mantle. They calculate NVE values using several seismic models: (1) they calculate NVE values using only the SMEAN seismic model (see figure 14 of ref. 10; 'Boschi-1' in Fig. 1), where hotspots with NVE ≥ 0.5 are treated as plumes, and hotspots with NVE < 0.5 are not plumes; (2) they also calculate NVE values for each hotspot by averaging the NVE values from five

different global seismic shear-wave models (including SMEAN), and this provides an additional method of identifying plume structures across several different seismic models ('Boschi-2' in Fig. 1).

We also use a third catalogue of mantle plumes from French and Romanowicz ref. 9 to distinguish between plume-fed and non-plume-fed hotspots. They identified 28 mantle plumes globally. Like the mantle plumes of ref. 10, not all of their plumes (see the legend to figure 4 in ref. 9) are continuous across the entire mantle. Their 'primary' plumes have $\delta V_s/V_s$ values that are less than -1.5% for most of the mantle between 1,000 km and 2,800 km; their 'clearly resolved' plumes are vertically continuous and have $\delta V_s/V_s > -0.5\%$ within the depth range 1,000–2,800 km; and their 'moderately resolved' plumes have $\delta V_s/V_s > -0.5\%$ over much of the depth range 1,000–2,800 km but are not as continuous as the primary and clearly resolved plumes. Therefore, like the plumes of ref. 10, the plumes of ref. 9 are assigned plume status based on the vertical continuity of the conduit across the mantle, and in both cases most plumes are not always observed to be completely continuous across the entire mantle.

The plume catalogues of refs 9 and 10 do not agree in every case (Fig. 1). For example, while the Boschi-2 plume catalogue (Fig. 1) and the F&R plume catalogue (Fig. 1) both identify a plume under the Galapagos, the Boschi-1 plume catalogue does not identify a plume beneath this hotspot. Additionally, out of the database of 38 hotspots with ^{3}He/^{4}He, the two Boschi plume catalogues[10] did not evaluate the presence or absence of plumes beneath six hotspots (Discovery, Manus Basin, Bouvet, Amsterdam–St Paul, Crozet, Ascension). Thus, of the 38 hotspots with ^{3}He/^{4}He data in Fig. 1 (see Supplementary Table 1), 32 hotspots were evaluated for the presence of mantle plumes in all three of the plume catalogues used here. Of these 32 hotspots, all three models are in agreement for 22 (or 69%) of the hotspots: under 18 hotspots all three models agree that there is a plume (Iceland, Hawaii, Samoa, Easter, Afar, Azores, Heard, Societies, Macdonald, Cape Verde, Marquesas, Reunion, Caroline, Pitcairn, Canary, Cameroon, Comores, Tristan-Gough), and under four hotspots all three models agree that there is no plume (Yellowstone, Cobb, Raton, Baja-Guadalupe) (see Fig. 1 and Supplementary Table 1). Thus, of the 32 hotspots with ^{3}He/^{4}He data that were analysed for the presence of plumes, just 10 hotspots (or 31%) show disagreement among the three plume catalogues. For 3 of the 10 hotspots (Darfur, Jan Mayen, Galapagos), two of the three plume catalogues identify a plume; for 7 of the 10 hotspots (Juan Fernandez, Meteor-Shona, Louisville, Hoggar, Marion, Eifel, St Helena), just one of the three plume catalogues identifies a plume.

Seismic velocity models for comparison with hotspot ^{3}He/^{4}He data. We use different global seismic shear-wave velocity models to evaluate relationships between the maximum ^{3}He/^{4}He values at hotspots and seismic velocity extracted at depth. First, we use an update of the composite SMEAN[25] model. SMEAN attempts to identify common mantle structure across different seismic shear-wave models. It is found to fit long-period seismic data at least as well as other tomographic models[61], and derived flow models typically provide the best fit to the geoid[62]. Using the original methods[25], we here combine more recent global seismic shear-wave models to generate an updated SMEAN, called SMEAN2. SMEAN2 has finer vertical sampling than SMEAN and combines S40RTS[63], GyPSum-S[64], and SAVANI[65]. The new SMEAN2 model is available at http://www-udc.ig.utexas.edu/external/becker/tdata.html.

The inverse relationship between the maximum ^{3}He/^{4}He values of plume-fed hotspots and shear-wave anomalies at 200 km is apparent for SMEAN and SMEAN2 (Fig. 3 and Extended Data Fig. 2). Seismic anomalies extracted from the individual seismic models used to generate the SMEAN2 model—S40RTS[63], GyPSum-S[64] and SAVANI[65]—are also compared with maximum ^{3}He/^{4}He values in Extended Data Fig. 2. Like SMEAN and SMEAN2, seismic anomalies extracted at 200 km depth from these constituent seismic models exhibit an inverse correlation with maximum ^{3}He/^{4}He. Because the seismic definition of plumes varies among the three different plume catalogues used here, we also explore the relationship between maximum ^{3}He/^{4}He and seismic velocity beneath plume-fed hotspots using each of the plume catalogues (Extended Data Fig. 2). We find that the inverse relationship between maximum ^{3}He/^{4}He at plume-fed hotspots and seismic velocity at 200 km (from different global seismic shear-wave velocity models) holds for all three seismic definitions of plumes (Fig. 3 and Extended Data Fig. 2).

However, seismic anomalies extracted from a recent global seismic model, SEMUCB-WM1[9], do not show the same clear relationship between maximum ^{3}He/^{4}He values and seismic velocity at 200 km depth (Extended Data Fig. 2). One reason for this may be that that SEMUCB-WM1 is of higher resolution than the other tomographic models, and so plume locations may be offset from the sampled hotspot locations, an effect that is less severe for the other, smoother models. We note that our conclusions are independent of SEMUCB-WM1 and do not rely on the plume classification scheme used (plume classification schemes from ref. 10 work equally well).

Seismic shear-wave velocity anomalies, as identified in the seismic models in Extended Data Fig. 2, vary up to about 6% at 200 km depth beneath hotspots. Lower shear-wave anomalies probably relate to increased temperature beneath hotspots, as low shear-wave velocity anomalies in the shallow mantle are associated with higher mantle temperatures[66]. Additionally, at the highest temperatures, partial melt may be present in the shallow upper mantle. Because the presence of partial melt can further reduce shear-wave velocity, partial melting in a volatile-rich asthenosphere associated with the hottest plumes may amplify the reduction in shear-wave velocity in the shallow mantle.

The Yellowstone hotspot. While some regional seismic studies hint at the presence of a plume beneath the Yellowstone hotspot[67,68], a Yellowstone plume is not visible in the global seismic models explored here. An important question is why the Yellowstone hotspot, which is not associated with a plume in any of the three plume catalogues, has relatively high maximum ^{3}He/^{4}He (19.4Ra; ref. 69). One possible explanation is that, while the high-^{3}He/^{4}He domain may be concentrated in the lower mantle and is preferentially sampled by plume-fed hotspots, pockets of high ^{3}He/^{4}He may exist in the upper mantle, possibly as plume relics left over from prior plume penetration into the upper mantle over geologic time. These relic high-^{3}He/^{4}He pockets may be sampled by non-plume hotspots sourced by the upper mantle. Indeed, among non-plume-fed hotspots with relatively high ^{3}He/^{4}He values, Yellowstone presents an unusual case. French and Romanowicz[9] suggested that a faint low-velocity conduit may underlie Yellowstone, but it is beyond the resolution of their study. Thus, the possibility remains that Yellowstone may actually relate to plume-fed volcanism. Nonetheless, the path of the putative Yellowstone plume would be complicated by interaction with the down-going Farallon slab[70,71], making it difficult to associate a deep plume conduit with surface expression of the hotspot.

Data availability. Source data for Figs 1–3 and Extended Data Figs 1–3 are provided with the online version of the paper. Data for the SMEAN2 seismic model used in the paper are shown in the source data (in Supplementary Table 1). The SMEAN2 model is available at http://www-udc.ig.utexas.edu/external/becker/tdata.html. The other seismic models shown in Extended Data Fig. 2 are published elsewhere, as indicated in the references cited.

31. Steinberger, B. Plumes in a convecting mantle: models and observations for individual hotspots. *J. Geophys. Res.* **105,** 11127–11152 (2000).
32. Courtillot, V., Davaille, A., Besse, J. & Stock, J. Three distinct types of hotspots in the Earth's mantle. *Earth Planet. Sci. Lett.* **205,** 295–308 (2003).
33. Macpherson, C., Hilton, D. R., Sinton, J. M., Poreda, R. J. & Craig, H. High ^{3}He/^{4}He ratios in the Manus backarc basin: implications for mantle mixing and the origin of plumes in the western Pacific Ocean. *Geology* **26,** 1007–1010 (1998).
34. Graham, D. W., Johnson, K. T. M., Priebe, L. D. & Lupton, J. E. Hotspot-ridge interaction along the Southeast Indian Ridge near Amsterdam and St. Paul Islands: helium isotope evidence. *Earth Planet. Sci. Lett.* **167,** 297–310 (1999).
35. Dunai, T. J. & Baur, H. Helium, neon, and argon systematics of the European subcontinental mantle: implications for its geochemical evolution. *Geochim. Cosmochim. Acta* **59,** 2767–2783 (1995).
36. Graham, D. W., Larsen, L. M., Hanan, B. B., Storey, M., Pedersen, A. K. & Lupton, J. E. Helium isotope composition of the early Iceland mantle plume inferred from the Tertiary picrites of West Greenland. *Earth Planet. Sci. Lett.* **160,** 241–255 (1998).
37. Starkey, N. A. *et al.* Helium isotopes in early Iceland plume picrites: constraints on the composition of high ^{3}He/^{4}He mantle. *Earth Planet. Sci. Lett.* **277,** 91–100 (2009).
38. Hilton, D. R., Grönvold, K., Macpherson, C. G. & Castillo, P. R. Extreme ^{3}He/^{4}He ratios in Iceland: constraining the common component in mantle plumes. *Earth Planet. Sci. Lett.* **173,** 53–60 (1999).
39. Marty, B., Pik, R. & Gezahegn, Y. Helium isotopic variations in Ethiopian plume lavas: nature of magmatic sources and limit on lower mantle contribution. *Earth Planet. Sci. Lett.* **144,** 223–237 (1996).
40. Scarsi, P. G. & Craig, H. Helium isotope ratios in Ethiopian Rift basalts. *Earth Planet. Sci. Lett.* **144,** 505–516 (1996).
41. Halldórsson, S. A., Hilton, D. R., Scarsi, P., Abebe, T. & Hopp, J. A common mantle plume source beneath the entire East African Rift System revealed by coupled helium-neon isotope systematics. *Geophys. Res. Lett.* **41,** 2304–2311 (2014).
42. Kurz, M. D., Jenkins, W. J. & Hart, S. R. Helium isotope systematics of ocean islands and mantle heterogeneity. *Nature* **297,** 43–47 (1982).
43. Kurz, M. D., Garcia, M. O., Frey, F. A. & O'Brien, P. A. Temporal helium isotopic variations within Hawaiian volcanoes: basalts from Mauna Loa and Haleakala. *Geochim. Cosmochim. Acta* **51,** 2905–2914 (1987).
44. Kurz, M. D., Curtice, J., Lott, D. E. III & Solow, A. Rapid helium isotopic variability in Mauna Kea shield lavas from the Hawaiian Scientific Drilling Project. *Geochem. Geophys. Geosyst.* **5,** Q04G14 (2004).
45. Valbracht, P. J., Staudacher, T., Malahoff, A. & Allègre, C. J. Noble gas systematics of deep rift zone glasses from Loihi Seamount, Hawaii. *Earth Planet. Sci. Lett.* **150,** 399–411 (1997).
46. Kurz, M. D., Meyer, P. S. & Sigurdsson, H. Helium isotopic systematics within the neovolcanic zones of Iceland. *Earth Planet. Sci. Lett.* **74,** 291–305 (1985).
47. Kurz, M. D. & Geist, D. Dynamics of the Galapagos hotspot from helium isotope geochemistry. *Geochim. Cosmochim. Acta* **63,** 4139–4156 (1999).
48. Graham, D. W., Christie, D. M., Harpp, K. S. & Lupton, J. E. Mantle plume helium in submarine basalts from the Galapagos platform. *Science* **262,** 2023–2026 (1993).
49. Jackson, M. G. *et al.* Globally elevated titanium, tantalum, and niobium (TITAN) in ocean island basalts with high ^{3}He/^{4}He. *Geochem. Geophys. Geosyst.* **9,** (2008).
50. Workman, R. *et al.* Recycled metasomatized lithosphere as the origin of the Enriched Mantle II (EM2) end member: evidence from the Samoan Volcanic Chain. *Geochem. Geophys. Geosyst.* **5,** Q04008 (2004).
51. Jackson, M., Kurz, M., Hart, S. & Workman, R. New Samoan lavas from Ofu island reveal a hemispherically heterogeneous high ^{3}He/^{4}He mantle. *Earth Planet. Sci. Lett.* **264,** 360–374 (2007a).
52. Poreda, R. J., Schilling, J.-G. & Craig, H. Helium isotope ratios in Easter Microplate basalts. *Earth Planet. Sci. Lett.* **119,** 319–329 (1993).
53. Stroncik, N., Niedermann, S., Schnabel, E. & Erzinger, J. Determining the geochemical structure of the mantle from surface isotope distribution patterns? Insights from Ne and He isotopes and abundance ratios. *AGU Fall Meet.* abstr. V51B–2519 (2011).
54. Honda, M. & Woodhead, J. D. A primordial solar-neon enriched component in the source of EM-I-type ocean island basalts from the Pitcairn Seamounts, Polynesia. *Earth Planet. Sci. Lett.* **236,** 597–612 (2005).
55. Garapić, G. *et al.* A radiogenic isotopic (He-Sr-Nd-Pb-Os) study of lavas from the Pitcairn hotspot: implications for the origin of EM-1 (enriched mantle 1). *Lithos* **228–229,** 1–11 (2015).
56. Jackson, M. G. *et al.* The return of subducted continental crust in Samoan lavas. *Nature* **448,** 684–687 (2007).
57. Graham, D. W., Humphris, S. E., Jenkins, W. J. & Kurz, M. D. Helium isotope geochemistry of some volcanic rocks from Saint Helena. *Earth Planet. Sci. Lett.* **110,** 121–131 (1992).
58. Hanyu, T. & Kaneoka, I. The uniform and low ^{3}He/^{4}He ratios of HIMU basalts as evidence for their origin as recycled materials. *Nature* **390,** 273–276 (1997).
59. Parai, R., Mukhopadhyay, S. & Lassiter, J. C. New constraints on the HIMU mantle from neon and helium isotopic compositions of basalts from the Cook–Austral Islands. *Earth Planet. Sci. Lett.* **277,** 253–261 (2009).
60. Hanyu, T., Tatsumi, Y. & Kimura, J.-I. Constraints on the origin of the HIMU reservoir from He–Ne–Ar isotope systematics. *Earth Planet. Sci. Lett.* **307,** 377–386 (2011).
61. Qin, Y., Capdeville, Y., Montagner, J.-P., Boschi, L. & Becker, T. W. Reliability of mantle tomography models assessed by spectral element simulation. *Geophys. J. Int.* **177,** 125–144 (2009).
62. Steinberger, B. & Calderwood, A. R. Models of large-scale viscous flow in the Earth's mantle with constraints from mineral physics and surface observations. *Geophys. J. Int.* **167,** 1461–1481 (2006).
63. Ritsema, J., van Heijst, H. J., Deuss, A. & Woodhouse, J. H. S40RTS: a degree-40 shear-velocity model for the mantle from new Rayleigh wave dispersion, teleseismic traveltimes, and normal-mode splitting function measurements. *Geophys. J. Int.* **184,** 1223–1236 (2011).
64. Simmons, N. A., Forte, A. M., Boschi, L. & Grand, S. P. GyPSuM: a joint tomographic model of mantle density and seismic wave speeds. *J. Geophys. Res.* **115,** (2010).
65. Auer, L., Boschi, L., Becker, T. W., Nissen-Meyer, T. & Giardini, D. Savani: a variable-resolution whole-mantle model of anisotropic shear-velocity variations based on multiple datasets. *J. Geophys. Res.* **119,** 3006–3034 (2014).
66. Stixrude, L. & Lithgow-Bertelloni, C. Mineralogy and elasticity of the oceanic upper mantle: origin of the low-velocity zone. *J. Geophys. Res.* **110,** B03204 (2005).
67. Yuan, H. & Dueker, K. Teleseismic P-wave tomogram of the Yellowstone plume. *Geophys. Res. Lett.* **32,** L07304 (2005).
68. Waite, G. P., Smith, R. B. & Allen, R. M. V_P and V_S structure of the Yellowstone hot spot from teleseismic tomography: evidence for an upper mantle plume. *J. Geophys. Res.* **111,** B04303 (2006).
69. Graham, D. W. *et al.* Mantle source provinces beneath the Northwestern USA delimited by helium isotopes in young basalts. *J. Volcanol. Geotherm. Res.* **188,** 128–140 (2009).
70. Kincaid, C., Druken, K., Griffiths, R. & Stegman, D. Bifurcation of the Yellowstone plume driven by subduction-induced mantle flow. *Nat. Geosci.* **6,** 395–399 (2013).
71. Leonard, T. & Liu, L. The role of a mantle plume in the formation of Yellowstone volcanism. *Geophys. Res. Lett.* **43,** (2016).
72. MacPherson, C. G., Hilton, D. R., Day, J. M. D., Lowry, D. & Grönvold, K. High-^{3}He/^{4}He, depleted mantle and low-δ^{18}O, recycled oceanic lithosphere in the source of central Iceland magmatism. *Earth Planet. Sci. Lett.* **233,** 411–427 (2005).
73. Kurz, M. D., Jenkins, W. J., Hart, S. R. & Clague, D. Helium isotopic variations in volcanic rocks from Loihi seamount and the island of Hawaii. *Earth Planet. Sci. Lett.* **66,** 388–406 (1983).
74. Moreira, M., Doucelance, R., Kurz, M. D., Dupré, B. & Allègre, C. J. Helium and lead isotope geochemistry of the Azores Archipelago. *Earth Planet. Sci. Lett.* **169,** 189–205 (1999).
75. Moreira, M. & Allègre, C. J. Rare gas systematics on Mid Atlantic Ridge (37-40°N). *Earth Planet. Sci. Lett.* **198,** 401–416 (2002).
76. Moreira, M., Kanzari, A. & Madureira, P. Helium and neon isotopes in São Miguel island basalts, Azores Archipelago: new constraints on the "low ^{3}He" hotspot origin. *Chem. Geol.* **322–323,** 91–98 (2012).

77. Hilton, D. R., Barling, J. & Wheller, G. E. Effect of shallow-level contamination on the helium isotope systematics of ocean-island lavas. *Nature* **373,** 330–333 (1995).

78. Farley, K. A., Basu, A. R. & Craig, H. He, Sr and Nd isotopic variations in lavas from Juan Fernandez Archipelago, SE Pacific. *Contrib. Mineral. Petrol.* **115,** 75–87 (1993).

79. Staudacher, T. & Allègre, C. J. Noble gases in glass samples from Tahiti: Teahitia, Rocard and Mehetia. *Earth Planet. Sci. Lett.* **93,** 210–222 (1989).

80. Moreira, M. & Allègre, C. J. Helium isotopes on the Macdonald seamount (Austral chain): constraints on the origin of the superswell. *C. R. Geosci.* **336,** 983–990 (2004).

81. Doucelance, R., Escrig, S., Moreira, M., Gariépy, C. & Kurz, M. D. Pb–Sr–He isotope and trace element geochemistry of the Cape Verde Archipelago. *Geochim. Cosmochim. Acta* **67,** 3717–3733 (2003).

82. Sarda, P., Moreira, M., Staudacher, T., Schilling, J.-G. & Allègre, C. J. Rare gas systematics on the southernmost Mid-Atlantic Ridge: constraints on the lower mantle and the Dupal source. *J. Geophys. Res.* **105,** 5973–5996 (2000).

83. Kurz, M. D., Le Roex, A. P. & Dick, H. J. B. Isotope geochemistry of the oceanic mantle near Bouvet triple junction. *Geochim. Cosmochim. Acta* **62,** 841–852 (1998).

84. Castillo, P. R., Scarsi, P. & Craig, H. He, Sr, Nd and Pb isotopic constraints on the origin of the Marquesas and other linear volcanic chains. *Chem. Geol.* **240,** 205–221 (2007).

85. Nicolaysen, K. P., Frey, F. A., Mahoney, J. J., Johnson, K. T. M. & Graham, D. W. Influence of the Amsterdam/St. Paul hot spot along the Southeast Indian Ridge between 77° and 88°E: correlations of Sr, Nd, Pb, and He isotopic variations with ridge segmentation. *Geochem. Geophys. Geosyst.* **8,** Q09007 (2007).

86. Breton, T. *et al.* Geochemical heterogeneities within the Crozet hotspot. *Earth Planet. Sci. Lett.* **376,** 126–136 (2013).

87. Graham, D. W., Lupton, J., Alberède, F. & Condomines, M. Extreme temporal homogeneity of helium isotopes at Piton de la Fournaise, Reunion Island. *Nature* **347,** 545–548 (1990).

88. Jackson, M.G., Price, A.A., Blichert-Toft, J., Kurz, M.D. & Reinhard, A. Geochemistry of lavas from the Caroline hotspot, Micronesia: evidence for primitive and recycled components in the mantle sources of lavas with moderately elevated $^3He/^4He$. *Chem. Geol.* http://dx.doi.org/10.1016/j.chemgeo.2016.10.038 (in the press).

89. Moreira, M., Staudacher, T., Sarda, P., Schilling, J.-G. & Allègre, C. J. A primitive plume neon component in MORB: the Shona ridge-anomaly, South Atlantic (51-52°S). *Earth Planet. Sci. Lett.* **133,** 367–377 (1995).

90. Hanyu, T. Deep plume origin of the Louisville hotspot: noble gas evidence. *Geochem. Geophys. Geosyst.* **15,** 565–576 (2014).

91. Graham, D. W., Hoernle, K. A., Lupton, J. E. & Schmincke, H. U. in *Shallow Level Processes in Ocean Island Magmatism: Distinguishing Mantle and Crustal Signatures* (eds Bohrson, W. A., Davidson, J. & Wolff, J. A.) 1–64 (Chapman Conference, American Geophysical Union, 1996).

92. Hilton, D. R., Macpherson, C. G. & Elliott, T. R. Helium isotope ratios in mafic phenocrysts and geothermal fluids from La Palma, the Canary Islands (Spain): implications for HIMU mantle sources. *Geochim. Cosmochim. Acta* **64,** 2119–2132 (2000).

93. Day, J. M. D. & Hilton, D. R. Origin of $^3He/^4He$ ratios in HIMU-type basalts constrained from Canary Island lavas. *Earth Planet. Sci. Lett.* **305,** 226–234 (2011).

94. Pik, R., Marty, B. & Hilton, D. R. How many mantle plumes in Africa? The geochemical point of view. *Chem. Geol.* **226,** 100–114 (2006).

95. Lupton, J. E., Graham, D. W., Delaney, J. R. & Johnson, H. P. Helium isotope variations in Juan De Fuca Ridge basalts. *Geophys. Res. Lett.* **20,** 1851–1854 (1993).

96. Schilling, J.-G., Kingsley, R., Fontignie, D., Poreda, R. & Xue, S. Dispersion of the Jan Mayen and Iceland mantle plumes in the Arctic: A He-Pb-Nd-Sr isotope tracer study of basalts from the Kolbeinsey, Mohns, and Knipovich Ridges. *J. Geophys. Res.* **104,** 10543–10569 (1999).

97. Debaille, V. *et al.* Primitive off-rift basalts from Iceland and Jan Mayen: Os-isotopic evidence for a mantle source containing enriched subcontinental lithosphere. *Geochim. Cosmochim. Acta* **73,** 3423–3449 (2009).

98. Reid, M. R. & Graham, D. W. Resolving lithospheric and sub-lithospheric contributions helium isotope variations in basalts from the southwestern US. *Earth Planet. Sci. Lett.* **144,** 213–222 (1996).

99. Franz, G., Steiner, G., Volker, F. & Pudlo, D. Plume related alkaline magmatism in Central Africa – the Meidob Hills (W. Sudan). *Chem. Geol.* **157,** 27–47 (1999).

100. Ammon, K., Dunai, T. J., Stuart, F. M., Meriaux, A.-S. & Gayer, E. Cosmogenic ^3He exposure ages and geochemistry of basalts from Ascension Island, Atlantic Ocean. *Quat. Geochronol.* **4,** 525–532 (2009).

101. Barfod, D. N., Ballentine, C. J., Halliday, A. N. & Fitton, J. G. Noble gases in the Cameroon line and the He, Ne, and Ar isotopic compositions of high (HIMU) mantle. *J. Geophys. Res.* **104,** 29,509–29,527 (1999).

102. Hanyu, T. *et al.* Isotope evolution in the HIMU reservoir beneath St. Helena: implications for the mantle recycling of U and Th. *Geochim. Cosmochim. Acta* **143,** 232–252 (2014).

103. Eiler, J. M. *et al.* Oxygen isotope variations in ocean island basalt phenocrysts. *Geochim. Cosmochim. Acta* **61,** 2281–2293 (1997).

104. O'Connor, J. M. & Jokat, W. Tracking the Tristan-Gough mantle plume using discrete chains of intraplate volcanic centers buried in the Walvis Ridge. *Geology* **43,** 715–718 (2015).

105. Hoernle, K. *et al.* How and when plume zonation appeared during the 132 Myr ago evolution of the Tristan Hotspot. *Nat. Commun.* **6,** 7799 (2015).

106. Hansen, S. E., Nyblade, A. A. & Benoit, M. H. Mantle structure beneath Africa and Arabia from adaptively parameterized P-wave tomography: implications for the origin of Cenozoic Afro-Arabian tectonism. *Earth Planet. Sci. Lett.* **319–320,** 23–34 (2012).
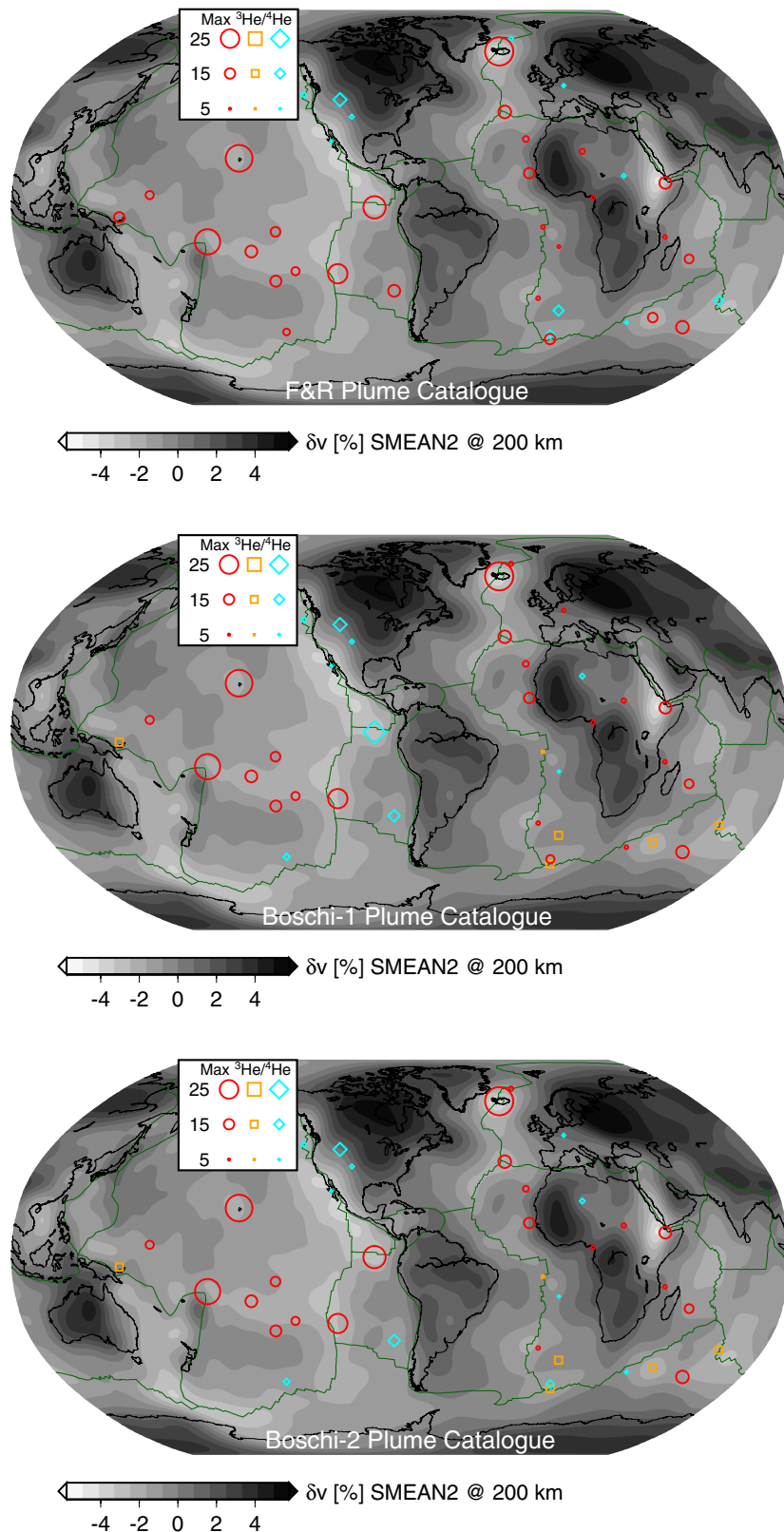
Extended Data Figure 1 | Maps showing the maximum ^{3}He/^{4}He at global hotspots. The magnitude of maximum ^{3}He/^{4}He values, for plume-fed (red circles) and non-plume-fed (cyan diamonds) hotspots, scale with the size of the symbol (see Supplementary Table 1). The scale shows the how the size of the symbol scales with the magnitude of the ^{3}He/^{4}He values, and shows 5Ra, 15Ra and 25Ra increments as examples. See the source data for this figure, in Supplementary Table 1, which cites refs 4, 9, 10, 19, 20, 24, 31–42, 45, 47–53, 55, 57, 58, 69, 72–106. Hotspots in Fig. 1 (see Supplementary Table 1) not evaluated for the presence of a plume

are represented by orange symbols. Three different methods are used to determine whether or not a hotspot is associated with a plume: the F&R plume catalogue[9] (top panel), the Boschi-1 plume catalogue[10] using SMEAN[25] (middle panel), and the Boschi-2 plume catalogue[10] that uses five different seismic models (bottom panel). The background of the maps is contoured (greyscale) based on seismic anomalies (δv) at 200 km for the SMEAN2 seismic model. The three panels use the same ^{3}He/^{4}He database (see Fig. 1 and Supplementary Table 1). The middle panel is also shown as Fig. 3.
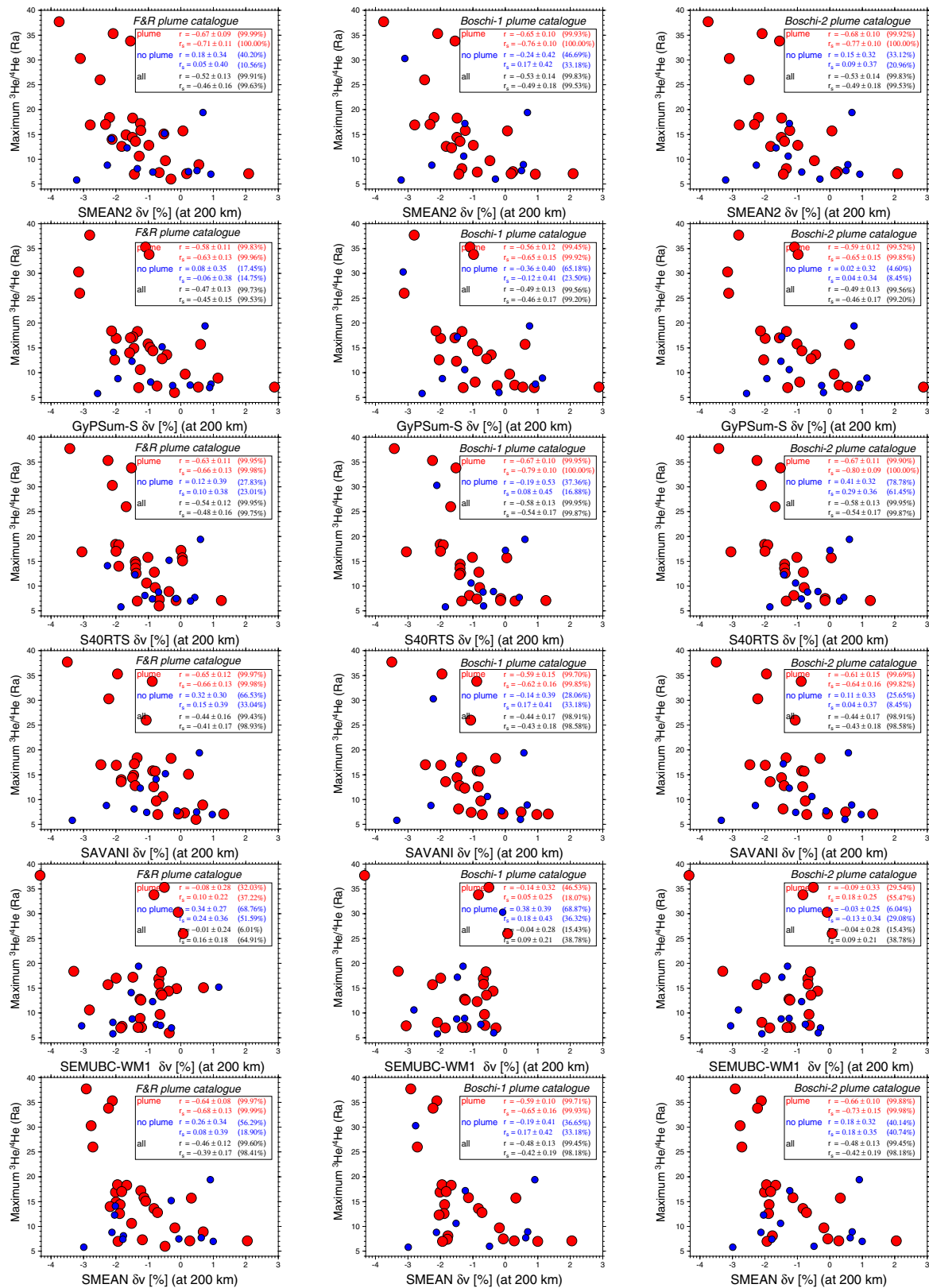
Extended Data Figure 2 | See next page for caption.

Extended Data Figure 2 | Maximum ^{3}He/^{4}He at hotspots compared with seismic velocity anomalies at 200 km. Data are taken from several global seismic models (SMEAN2, GyPSum-S[64], S40RTS[63], SAVANI[65], SEMUCB-WM1[9] and SMEAN[25]) and three plume classification schemes from refs 9 and 10. See the source data for this figure, in Supplementary Table 1, which cites refs 4, 9, 10, 19, 20, 24, 31–42, 45, 47–53, 55, 57, 58, 69, 72–106. The Pearson (r) and Spearman rank (r_S) correlation coefficients are provided in the panels and are calculated from individual observations for plume-fed hotspots (for the red symbols only), non-plume-fed hotspots (blue symbols), and all hotspots (red and blue symbols); the text in boxes provides information about correlation coefficients for plume-fed hotspots only (red text), non-plume-fed hotspots only (blue text), and all hotspots (black text). Spearman correlation coefficients provide more reliable estimates of correlation in the presence of nonlinear relationships, but results for r and r_S are generally consistent. To evaluate the actual statistical relevance of the correlations, the 1σ uncertainty is provided (calculated using bootstrap), as is the significance level of the correlation coefficients; this P value (in parentheses, given in per cent) is calculated with Student's t-test assuming normally distributed data. In each panel, the presence or absence of a plume depends on the plume catalogue used (see Fig. 1 and Supplementary Table 1): The left panels use the F&R plume catalogue[9] (Fig. 1); the middle panels use the Boschi-1 plume catalogue[10], which has normalized vertical extent values NVE ≥ 0.5 as derived from the SMEAN model (Fig. 1); the right panels use the Boschi-2 plume catalogue[10], which relies on the average NVE calculated from five different seismic models (Fig. 1), and defines plumes as having NVE ≥ 0.5. The sample sizes for the Boschi-1, Boschi-2 and F&R plume catalogues are as follows: Boschi-1 ($n = 23$ plumes, $n = 9$ non-plumes), Boschi-2 ($n = 21$ plumes, $n = 11$ non-plumes), F&R ($n = 27$ plumes, $n = 11$ non-plumes). All panels use the same ^{3}He/^{4}He database (see Supplementary Table 1). The panels showing SMEAN2 seismic anomalies at 200 km for the Boschi-1 and -2 plume catalogues[10] are also shown as Fig. 3.
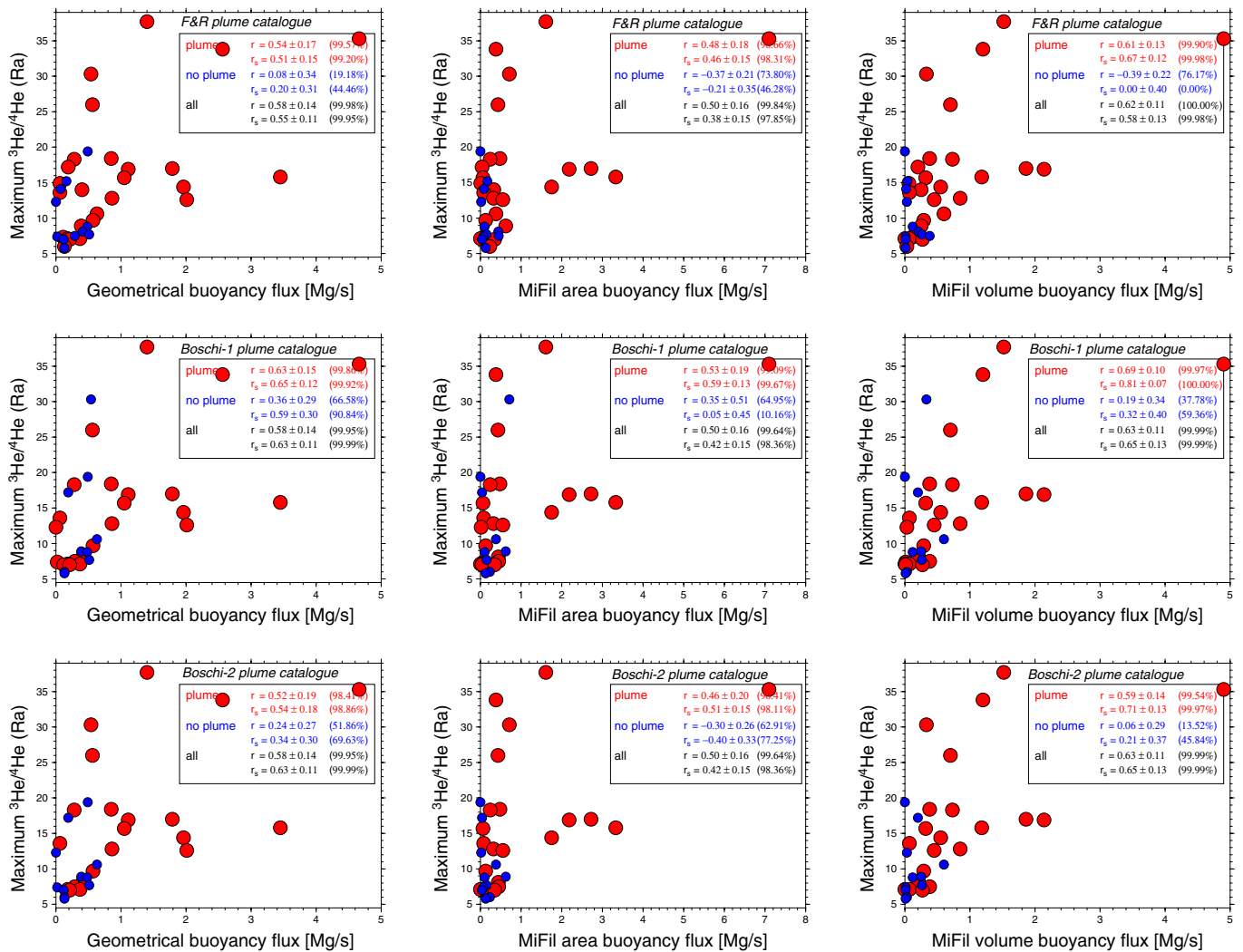
Extended Data Figure 3 | Maximum ^{3}He/^{4}He at hotspots versus hotspot buoyancy flux. Correlation values and plume selection as in Extended Data Fig. 2. See the source data for this figure, in Supplementary Table 1, which cites refs 4, 9, 10, 19, 20, 24, 31–42, 45, 47–53, 55, 57, 58, 69, 72–106. Hotspot buoyancy flux models are from ref. 24, and include the 'geometrical' hotspot buoyancy flux, the 'MiFil area' buoyancy flux, and the 'MiFil volume' buoyancy flux. Because hotspot buoyancy fluxes are not available for the Manus Basin locality, the sample sizes for the Boschi-1, Boschi-2 and F&R plume catalogues are as follows: Boschi-1 ($n = 23$ plumes, $n = 9$ non-plumes), Boschi-2 ($n = 21$ plumes, $n = 11$ non-plumes), F&R ($n = 26$ plumes, $n = 11$ non-plumes). The panels showing MiFil volume hotspot buoyancy flux for the Boschi-1 and -2 plume catalogues[10] are also shown in Fig. 3.